SCIENCE CHINA
Life Sciences

•COVER ARTICLE•

September 2022 Vol.65 No.9: 1685–1700
https://doi.org/10.1007/s11427-022-2155-0

H3K27me3 shapes DNA methylome by inhibiting UHRF1-mediated H3 ubiquitination

Honglian Zhang[1†], Ying Liu[1,2†], Yali Xie[1,2†], Yunji Zhu[1,2†], Jingwen Liu[1,2] & Falong Lu[1,2*]

[1]*State Key Laboratory of Molecular Developmental Biology, Institute of Genetics and Developmental Biology, Innovative Academy of Seed Design, Chinese Academy of Sciences, Beijing 100101, China;*
[2]*University of Chinese Academy of Sciences, Beijing 100049, China*

Received June 22, 2022; accepted June 27, 2022; published online July 11, 2022

DNA methylation and histone lysine tri-methylation at H3K27 (H3K27me3) are two chromatin modifications for transcriptional gene silencing, which play important roles in diverse biological processes, including cell fate determination and cell lineage commitment. These two marks are largely mutually exclusive and target distinct sets of genes in the mammalian genome. However, how H3K27me3 shapes the DNA methylome remains elusive. Here, we report that the loss of H3K27me3 modification leads to increased DNA methylation at previously marked H3K27me3 sites, indicating that H3K27me3 negatively regulates DNA methylation. Genome-wide analysis of H3 ubiquitination, essential for recruitment and activation of DNA methyltransferase DNMT1, reveals the absence of H3 ubiquitination at H3K27me3 marked nucleosomes. Moreover, loss of H3K27me3 modification induces an increase in H3K18 ubiquitination at the corresponding hyper-methylated loci. Importantly, we show that H3K27me3 directly inhibits UHRF1-mediated H3 ubiquitination toward nucleosomes in a defined biochemical assay. Taken together, our findings reveal a general mechanism for H3K27me3-mediated shaping of the mammalian DNA methylome via modulation of H3 ubiquitination.

DNA methylation, H3K27me3, UHRF1, Polycomb, H3 ubiquitination

Citation: Zhang, H., Liu, Y., Xie, Y., Zhu, Y., Liu, J., and Lu, F. (2022). H3K27me3 shapes DNA methylome by inhibiting UHRF1-mediated H3 ubiquitination. Sci China Life Sci 65, 1685–1700. https://doi.org/10.1007/s11427-022-2155-0

INTRODUCTION

DNA methylation is the covalent addition of methyl groups to the cytosine of CpG dinucleotides, and is associated with numerous biological processes including the regulation of gene expression, silencing of transposable elements, genomic imprinting, and X-chromosome inactivation (Disteche and Berletch, 2015; Elhamamsy, 2017; Li and Zhang, 2014). Aberrations in DNA methylation levels and patterns have been associated with various diseases, such as cancer and developmental disorders (Amir et al., 1999; Brookes and Shi, 2014; Hon et al., 2012). Cytosine methylation is achieved through the activities of both *de novo* and maintenance methyltransferases (Chen and Zhang, 2020). New DNA methylation patterns are established by DNMT3 family enzymes including DNMT3A, DNMT3B, and DNMT3C (Barau et al., 2016; Chen and Zhang, 2020; Goll and Bestor, 2005; Jain et al., 2017; Okano et al., 1999). DNMT1 and UHRF1 are well-established as essential proteins for DNA methylation maintenance (Bostick et al., 2007; Sharif et al., 2007). However, recent studies have revealed that DNMT1 and UHRF1 can also mediate *de novo* DNA methylation (Li et al., 2018a; Schmitz et al., 2019; Wang et al., 2020).

H3K27me3 modification is an epigenetic mark strongly linked to gene silencing (Cao and Zhang, 2004; Chittock et

†Contributed equally to this work
*Corresponding author (email: fllu@genetics.ac.cn)

al., 2017; Simon and Kingston, 2009), and is catalyzed by Polycomb Repressive Complex 2 (PRC2), which consists of three core components, EZH1/2 (EZH1 or EZH2), EED, and SUZ12 (Laugesen et al., 2019). H3K27me3 has been characterized as a primary mechanism for epigenetic regulation of cell identity via repression of key developmental genes that do not need to be expressed in the current cell fate (Margueron and Reinberg, 2011). Tight regulation of H3K27me3 is essential for normal development and abnormalities in this epigenetic process lead to diverse defects (Hirabayashi et al., 2009; Margueron et al., 2008; Miró et al., 2009; Schwartzentruber et al., 2012; Wu et al., 2012; Yu et al., 2019; Yu et al., 2017; Zhao and Wu, 2021). In mammals, most of the genomic CpG sites are methylated by default, while selected regions are hypo-methylated in a highly regulated, cell type-specific manner (Stadler et al., 2011). H3K27me3 marked regions are among the most well-known regions to be hypo-methylated (Brinkman et al., 2012). Consistent with epigenomic observations, proteomic and single-molecule analyses have also indicated that DNA methylation and H3K27me3 modification rarely co-exist in chromatin (Bartke et al., 2010; Li et al., 2018b; Murphy et al., 2013; Yang et al., 2018).

As DNA methylation and H3K27me3 are two epigenetic gene silencing marks essential for cell fate determination and development, uncovering the mechanisms that regulate their antagonism remains a topic of considerable ongoing interest. Several studies have revealed that loss of DNA methylation leads to H3K27me3 redistribution from Polycomb targets to other regions (Brinkman et al., 2012; Reddington et al., 2013; Wu et al., 2010). This can be partially explained by the fact that DNA methylation on nucleosomes can inhibit PRC2 binding (Wu et al., 2010). One study have reported that the loss of H3K27me3 alter the DNA methylation at a limited number of promoters in mESCs using methylated DNA immuno-precipitation (MeDIP), a relatively low-resolution approach (Hagarman et al., 2013). So, whether and how H3K27me3 affects DNA methylation remains elusive.

Here, we reveal that H3K27me3 negatively regulates DNA methylation by showing elevated DNA methylation in regions previously bearing H3K27me3 marks in the absence of H3K27me3. Mechanistically, H3K18ub, which is essential for DNMT1 recruitment and activity, is inhibited by H3K27me3. This is achieved by inhibition of UHRF1-mediated H3 ubiquitination activity by H3K27me3 modification on the nucleosomes. Our study thus reveals the regulation of DNA methylation by H3K27me3 through a third chromatin modification, H3 ubiquitination, mediated by UHRF1, highlighting the complex cross-regulation between chromatin modifications.

RESULTS

H3K27me3 anti-correlates with DNA methylation

In order to confirm whether H3K27me3 anti-correlation with DNA methylation is a general feature in different cell types, we investigated the relationship between H3K27me3 and DNA methylation in several different tissues and cell lines. Examination of a panel of methylomes and H3K27me3 sites in three mouse tissues and three human tissues (Bernstein et al., 2010; Consortium, 2012; Hawkins et al., 2010; Lister et al., 2009; Lister et al., 2011; Micheletti et al., 2017; Ramírez et al., 2016; Schultz et al., 2015) revealed that DNA methylation was generally depleted at H3K27me3-enriched sites (Figure 1A). H3K27me3-enriched sites in the methylomes of HeLa human cancer cells and E14 mouse embryonic stem cells (mESCs) were also checked. We found that DNA methylation was depleted at H3K27me3-enriched loci genome wide in these cell lines as seen in tissues (Figure 1B and C). These data confirm that the hypo-methylation of H3K27me3 marked sites is a general feature conserved in mouse and human.

Increased DNA methylation at previously marked H3K27me3 sites in the absence of H3K27me3

We hypothesize that DNA methylation will increase at previously marked H3K27me3 sites following H3K27me3 depletion, if H3K27me3 indeed negatively regulates DNA methylation. To test the hypothesis, we generated HeLa cells carrying CRISPR/Cas9-mediated loss-of-function deletions in the *SUZ12* gene (Wang et al., 2013), which encodes a core component of the PRC2 complex required for H3K27me3 establishment (Højfeldt et al., 2018) (Figure S1A, Tables S1 and S2 in Supporting Information). We obtained two independent *SUZ12* knock out (KO) HeLa cell lines that exhibited depletion of SUZ12 as well as H3K27me3 (Figure 2A and Figure S1 in Supporting Information). Using whole genome bisulfite sequencing (WGBS), we observed an obvious increase in DNA methylation at the majority of previously marked H3K27me3 sites in the *SUZ12* KO cells (Figure 2B). The median DNA methylation level increased from approximately 30.8% to 41.4% at all the previously marked sites in the absence of H3K27me3, whereas methylation levels were minimally affected outside of the previously marked H3K27me3 sites (Figure 2C and D).

There were 3,714 hyper-methylated Differential Methylation Regions (hyper-DMRs) genome-wide in the *SUZ12* KO HeLa cells. Notably, we found that 93.07% of the hyper-DMRs overlapped with previously marked H3K27me3 sites (Figure 2E, left panel), again confirming that a preferential increase in DNA methylation occurred at previously marked H3K27me3 sites resulting from *SUZ12* KO. This finding represents a significant enrichment of DNA hyper-methy-

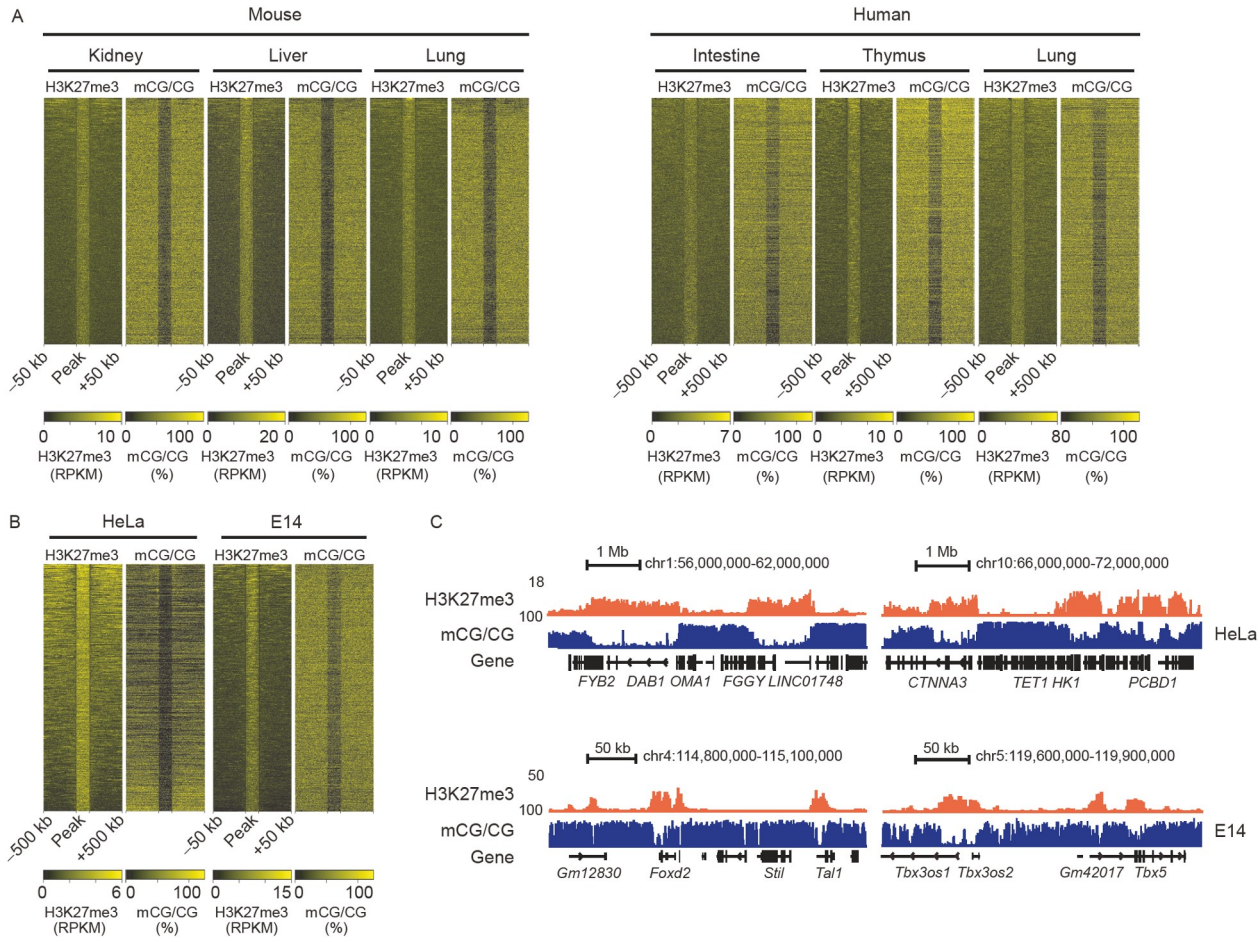

Figure 1 H3K27me3 anti-correlates with DNA methylation. A, Heatmaps representing the corresponding levels of DNA methylation around H3K27me3 peaks. Each row represents one H3K27me3 peak and shows H3K27me3 ChIP-seq signal intensity (RPKM) and average DNA methylation level at H3K27me3 peak ± 50 kb in mouse tissues or ±500 kb in human tissues. H3K27me3 ChIP-seq and WGBS data are from the GEO database as detailed in the methods. B, Heatmaps are presented the same way as that in A, except in HeLa and E14 cells. C, Genome browser tracks showing anti-correlation between H3K27me3 modification and DNA methylation in representative regions of HeLa and E14 genomes.

lated sites in H3K27me3 marked regions, considering that H3K27me3 marks cover 30.78% of the HeLa genome (Figure 2E, right panel). These results therefore indicate that the loss of H3K27me3 induces an increase of DNA methylation at previously marked H3K27me3 sites, suggesting that DNA methylation is negatively regulated by H3K27me3.

We also constructed *Suz12* KO in mESC E14 cells and obtained two independent KO cell lines that exhibited depletion of SUZ12 as well as H3K27me3 (Figure S2A–C in Supporting Information). We were thus able to see that DNA methylation increased at the majority of previously marked H3K27me3 sites in *Suz12* KO E14 cells (Figure S3A and B in Supporting Information). Moreover, we identified 5,507 hyper-DMRs in the *Suz12* KO E14 cells, among which 19.47% overlapped with previously marked H3K27me3 sites (Figure S3C, left panel in Supporting Information), a significant enrichment compared with the overall 6.62% of H3K27me3 marked regions in the E14 genome (Figure S3C, right panel in Supporting Information). We noticed that loss of H3K27me3 led to a greater degree of DNA methylation level increase at H3K27me3 marked sites in HeLa cells than in E14 cells (HeLa cells: from 30.8% to 41.4%; E14 cells: from 63.21% to 63.8%) (Figure 2B and C, Figure S3A in Supporting Information), although the enrichment ratio of DMRs overlapped with H3K27me3 was comparable in these two cell lines (HeLa cells: 93.07%/30.78%=3.02; E14 cells: 19.47%/6.62%=2.94) (Figure 2E and Figure S3C in Supporting Information). This may be related to complex DNA methylation regulation by DNMT1, DNMT3 family proteins, as well as TET proteins in E14 cells. Therefore, to better study the mechanism of H3K27me3 in regulating DNA methylation, we mainly focused on the HeLa cells in the subsequent study.

DNA methylation increase at previously marked H3K27me3 sites is independent of transcriptomic changes induced by *SUZ12* KO

Both DNA methylation and H3K27me3 epigenetic marks are well-known to silence gene expression (Yu et al., 2019). In

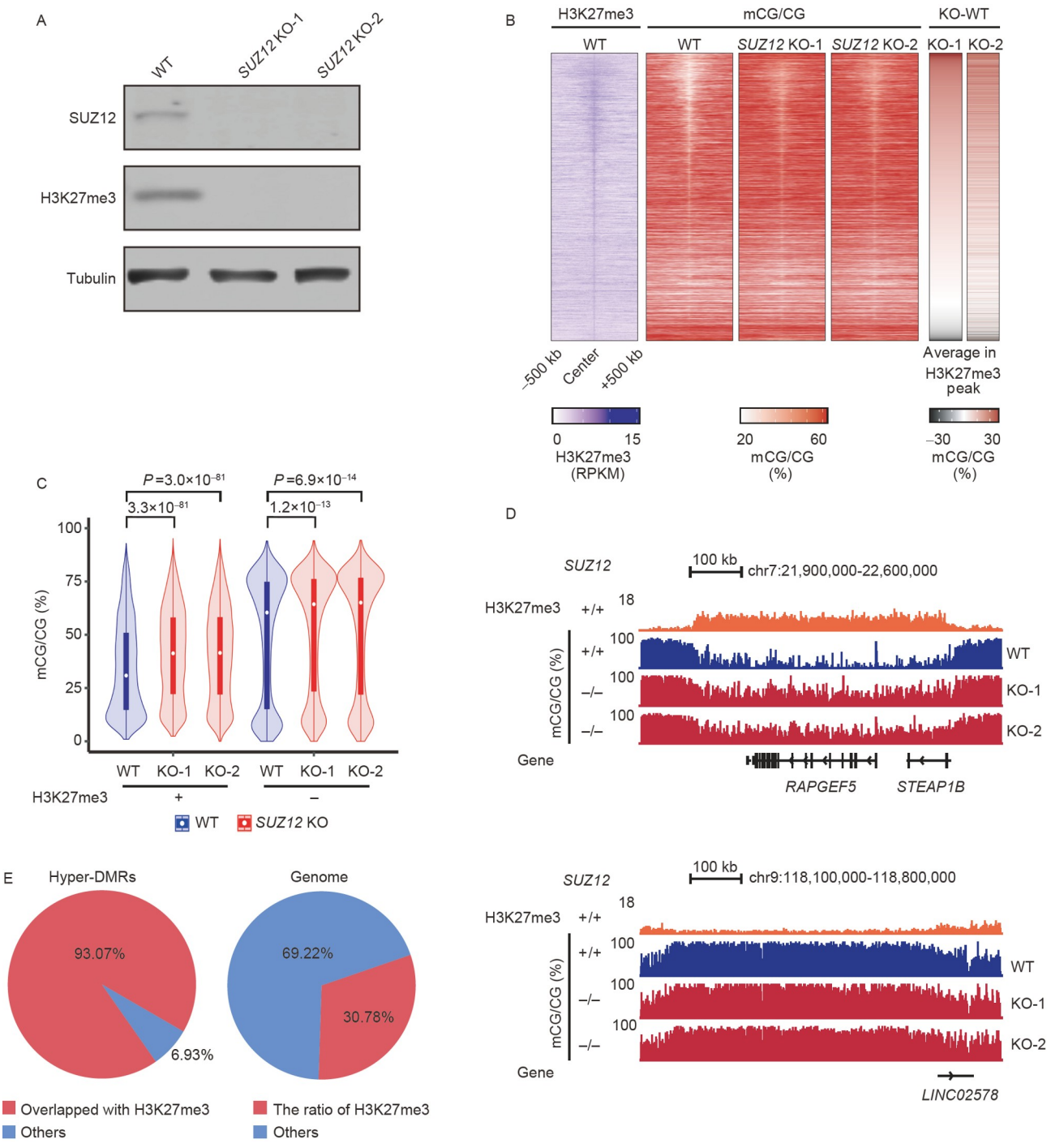

Figure 2 Loss of H3K27me3 modification induces an increase in DNA methylation at previously marked H3K27me3 sites in HeLa cells. A, Western blots of SUZ12 and H3K27me3 in WT and *SUZ12* KO HeLa cells. Tubulin is used as a loading control. B, Heatmaps representing the corresponding levels of DNA methylation and H3K27me3 enrichment (RPKM) in WT and *SUZ12* KO HeLa cells (2 clones) at H3K27me3 peak sites. H3K27me3 peaks are sorted by total H3K27me3 signals around the peak center. The differences indicate the average methylation levels in *SUZ12* KO cells subtracted from those in WT cells at each H3K27me3 peak. C, Violin plots showing the levels of DNA methylation in WT and *SUZ12* KO HeLa cells. The outer shape indicates the distribution across all regions. The center dot indicates the median average value. The box represents the interquartile range. Paired *t*-test is used to determine *P* values. D, Genome browser tracks showing the changes in CpG methylation levels at H3K27me3-marked and -unmarked sites in WT and *SUZ12* KO HeLa cells. E, Pie chart showing the distribution of hyper-DMRs in *SUZ12* KO HeLa cells in previously marked H3K27me3 regions (left panel). Pie charts show the percentage of H3K27me3 modification in the genome of HeLa cells (right panel). P=5.73e^{-238} (Fisher's exact test). Hyper-DMRs are identified by methpipe-3.4.3. The merged DMRs of two clones are used in E.

light of our results showing increased DNA methylation in the *SUZ12* KO cells, we performed RNA-seq in WT and two *SUZ12* KO HeLa cells to assess the transcriptional changes at these regions. The RNA-seq data of the two clones were

highly reproducible (Figure S4A in Supporting Information), thus we then pooled data with replicates in the subsequent analysis. We found that depletion of SUZ12 led to 313 differentially up-regulated genes and 15 differentially down-regulated genes with a fold change >2 cut-off (Figure S4B, Table S3 in Supporting Information). Among the 313 up-regulated genes, 189 genes were located within previously marked H3K27me3 peaks, and 214 genes overlapped with hyper-DMRs in *SUZ12* KO cells (Figure S4C, left panel in Supporting Information). However, among the 15 down-regulated genes, only 2 genes overlapped with H3K27me3 peaks, and 4 genes overlapped with hyper-DMRs (Figure S4C, right panel in Supporting Information). These numbers were considerably lower than the 4,751 protein coding genes marked by H3K27me3 in HeLa cells. Therefore, loss of H3K27me3 causes up-regulation of a small number of genes in HeLa cells, suggesting that the global changes in DNA methylation we observed at previously marked H3K27me3 sites were not likely a result of transcriptional changes related to *SUZ12* KO.

H3K27me3 anti-correlates with H3K18ub

As shown in previous studies, DNMT1, but not DNMT3A/3B which is minimally expressed, provides the primary contribution to DNA methylation in HeLa cells (Palii et al., 2008). DNMT1 targeting and activity *in vivo* is regulated by UHRF1. UHRF1 recognizes hemi-methylated DNA through its SET and RING-associated (SRA) domain and ubiquitinates the histone H3 tail at K18 and K23 (Arita et al., 2008; Bostick et al., 2007; Hashimoto et al., 2008; Ishiyama et al., 2017; Liu et al., 2013; Nishiyama et al., 2013; Qin et al., 2015; Sharif et al., 2007). Then the ubiquitinated H3 can recruit and stimulate the activity of DNMT1 to methylate the target DNA (Nishiyama et al., 2013; Qin et al., 2015). In this process, the ubiquitination of H3K18 or H3K23 serves as a key step in DNMT1-mediated DNA methylation. Considering that H3K27me3 modification is very close to the K18 and K23 sites modified by UHRF1 in the N-terminal tail of H3, we hypothesized that H3K27me3 potentially antagonizes DNA methylation through regulating UHRF1-mediated H3 ubiquitination.

To test this hypothesis, we first asked whether H3K18ub and H3K23ub were depleted at H3K27me3 marked sites. Since no commercially available antibodies have yet been developed for H3K18ub, and commercial H3K23ub antibody is only applicable for western blots, we therefore generated a rabbit antibody against H3K18ub. In order to determine the specificity of the antibody, we tried to generate *UHRF1* KO in HeLa cells and *Uhrf1* KO in E14 cells. Unfortunately, we were unable to get the homozygous *UHRF1* KO cell lines after screening more than 400 CRISPR/Cas9 clones, potentially because hypo-methylation mediated by *UHRF1* KO is lethal in HeLa cells, similar to the lethal phenotype reported for *DNMT1* KO (Bostick et al., 2007; Elliott et al., 2016). But we successfully constructed *Uhrf1* KO in E14 cells by large fragment deletion of the UHRF1 coding region (Figure S5A and B, Tables S1, S2 in Supporting Information), for which DNA methylation has been shown to be inessential for cell survival (Tsumura et al., 2006). Our H3K18ub antibody successfully detected one band at the expected size in WT E14 mESCs which was clearly diminished in *Uhrf1* KO cells, thereby demonstrating its specificity against UHRF1-dependent H3 ubiquitination (Figure 3A and Figure S5C). Immuno-staining also confirmed its dependence of UHRF1 (Figure 3B). To gain further confirmation of the specificity of the antibody, we performed chromatin immuno-precipitation coupled with next-generation sequencing (ChIP-seq) experiments using this antibody in WT and *Uhrf1* KO E14 cells. The two replicates of H3K18ub ChIP-seq data in WT and *Uhrf1* KO E14 cells were highly reproducible (Figure S5D in Supporting Information), thus we then used 74,299 overlapping peaks of replicates in WT E14 cells for the subsequent analysis. And we found that the H3K18ub peaks in E14 cells were almost completely abolished in *Uhrf1* KO cells (Figure 3C and Figure S5E in Supporting Information). Since tests of commercial H3K23ub antibody failed in ChIP-seq, we therefore relied on our custom H3K18ub antibody in subsequent H3 ubiquitination analyses in this study.

Then we performed H3K18ub ChIP-seq in WT HeLa cells, and the two replicates of H3K18ub ChIP-seq data were also highly reproducible (Figure S6A in Supporting Information). 2,641 overlapping peaks of replicates in WT HeLa cells were analyzed and characterized. First, we found that H3K18ub peaks in HeLa cells mainly localized in distal intergenic, promoter and other exon (35.14%, 29.61% and 13.44% respectively) (Figure S6B, left panel in Supporting Information). To gain further insights into the enrichment of H3K18ub peaks in genome, these peaks were compared with random peaks with the same length of the corresponding genome and showed a enrichment at intergenic enhancer (Figure S6B, right panel in Supporting Information), which may be related to the aberrant DNA methylation of enhancer in cancer cells (Aran and Hellman, 2013; Aran et al., 2013; Bell et al., 2016; Brocks et al., 2014).

If H3K27me3 indeed antagonizes DNA methylation through regulating H3 ubiquitination, H3 ubiquitination would be absent in H3K27me3 marked nucleosomes. To test the hypothesis, we analyzed the H3K18ub or H3K27me3 enrichment at H3K27me3 or H3K18ub marked sites respectively in HeLa and E14 WT cells, the results indicated that the H3K18ub signal at H3K27me3 marked regions was negligible or undetectable, and H3K27me3 modification was absent in the H3K18ub marked regions (Figure 3D and E), suggesting that H3K27me3 may anti-correlate H3K18ub

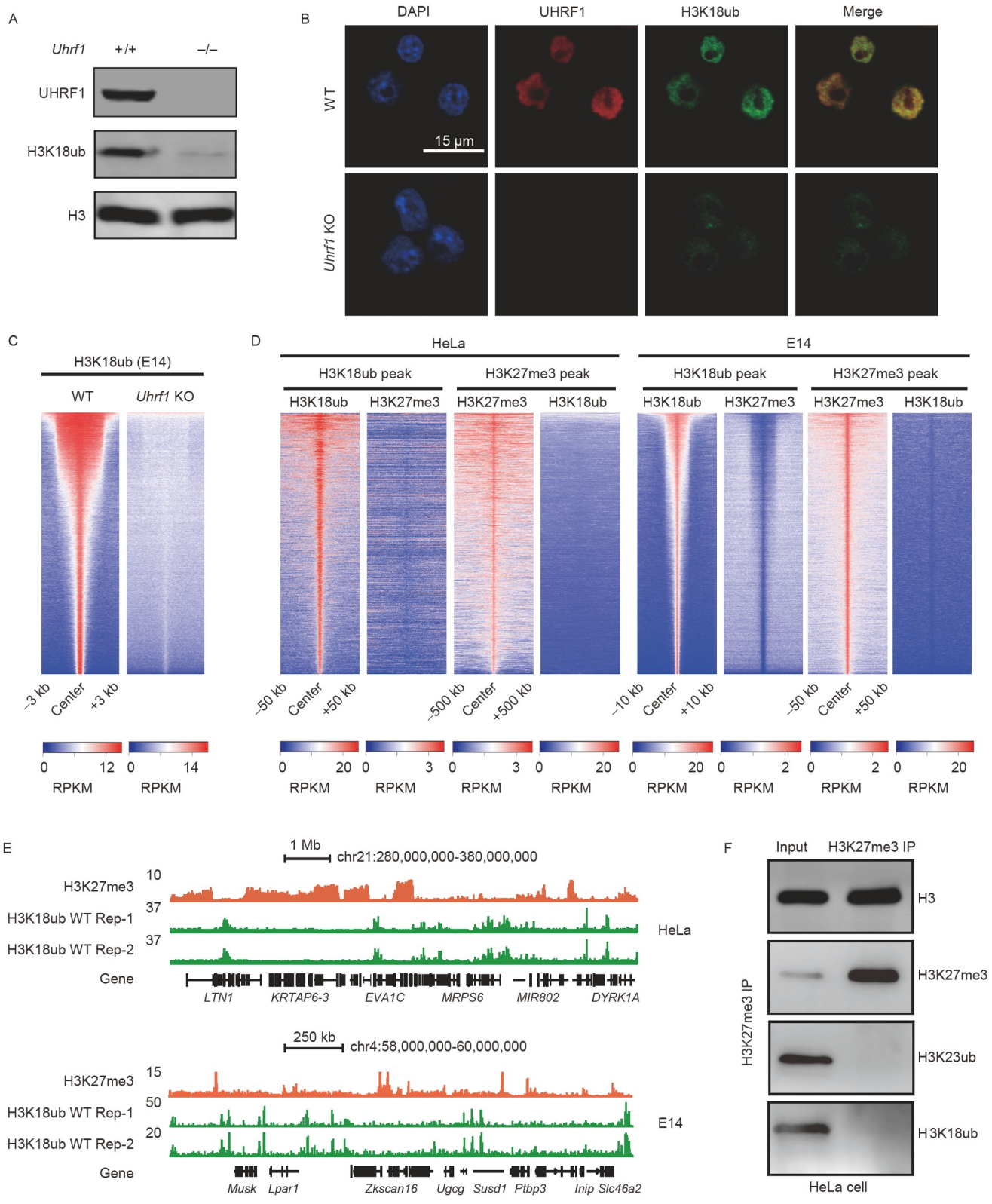

Figure 3 H3K27me3 modification anti-correlates with H3K18ub modification. A, Western blots of UHRF1 and H3K18ub in WT and *Uhrf1* KO E14 cells. H3 is used as a loading control. B, Immuno-staining showing co-localization of H3K18ub with UHRF1 in E14 cells and diminished signal in *Uhrf1* KO E14 cells. Scale bar: 15 μm. C, Heatmap showing the enrichment of H3K18ub modification in WT and *Uhrf1* KO E14 cells. Each row represents H3K18ub ChIP-seq signal intensity (RPKM) at H3K18ub peaks in WT cells (± 3 kb). D, Heatmap showing the levels of H3K27me3 signals at H3K18ub sites overlapped in two replicates and H3K18ub signals at H3K27me3 sites in HeLa and E14 cells. The merged H3K18ub ChIP-seq data of two replicates are shown in C and D. E, Genome browser tracks showing anti-correlation between H3K18ub and H3K27me3 in HeLa and E14 cells. F, Histone H3 from HeLa cells is immunoprecipitated using antibody against H3K27me3. H3 modifications are analyzed by western blot.

genome wide. To further test if UHRF1-mediated H3 ubiquitination is depleted in H3K27me3 marked nucleosomes, we performed immuno-precipitation in HeLa cells using antibody specific for H3K27me3 and blotted with H3K18ub and H3K23ub. The results clearly demonstrated that H3K18ub and H3K23ub were depleted from H3 with H3K27me3 modification (Figure 3F). Taken together, our data reveal that UHRF1-mediated H3 ubiquitination is absent in H3K27me3 marked nucleosomes.

H3K18ub marks increase at previously marked H3K27me3 sites in the absence of H3K27me3

Next, we ask whether the loss of H3K27me3 marks leads to the increase of H3K18ub marks at the H3K27me3 targeting sites using H3K18ub ChIP-seq in WT and *SUZ12* KO HeLa cells. This analysis identified 2,641 overlapping H3K18ub peaks of two replicates in WT and 5,106 overlapping H3K18ub peaks of two replicates in *SUZ12* KO HeLa cells, among which 2,246 WT peaks (85%) overlapped with peaks in *SUZ12* KO cells (Figure 4A and Figure S6A in Supporting Information). In order to better understand and quantify the changes in peak signals between WT and *SUZ12* KO cells, we analyzed the H3K18ub peak signal (RPKM, Reads Per Kilobase per Million mapped reads) ratio (KO/WT) with fold change cut-off values of >1.5, 2, 3, or 4. This analysis revealed that 2,360, 1,011, 350, and 161 H3K18ub peaks increased at those respective cut-offs among 5,106 peaks in *SUZ12* KO cells, while 276, 38, 3, and 2 peaks decreased at those respective cut-offs among the 5,487 combined H3K18ub peaks in WT and *SUZ12* KO cells. These results thus further confirm that loss of H3K27me3 marks leads to an increase in H3K18ub signal in HeLa cells.

To determine whether the increase in H3K18ub marks in *SUZ12* KO cells was associated with H3K27me3 marked loci in WT cells, we first examined the ratio of H3K18ub peaks that overlapped with H3K27me3 marked sites. This analysis showed that among the 5,106 H3K18ub peaks in *SUZ12* KO cells, 595 peaks (11.65%) overlapped with H3K27me3 sites, while only 72 (2.73%) out of 2,641 H3K18ub peaks overlapped with H3K27me3 sites in the WT background (Figure 4B). Moreover, among 3,025 H3K18ub peaks unique to *SUZ12* KO cells, 17.26% overlapped with H3K27me3 sites, indicating that the H3K18ub peaks acquired following depletion of H3K27me3 marks were enriched specifically at the previously marked H3K27me3 sites. We then compared the average H3K18ub peak signal ratio (KO/WT) between H3K18ub peaks that overlapped with H3K27me3 (595) sites with those non-overlapped (4,511) with H3K27me3 sites. We observed that peaks overlapped with H3K27me3 sites showed a much greater increase in H3K18ub signal compared to those not overlapped with H3K27me3 in cells depleted for H3K27me3 marks (Figure 4C).

To further confirm the correlation between increased H3K18ub modification and the absence of H3K27me3 modification in the *SUZ12* KO background, we compared the degree of increase in H3K18ub modification between H3K18ub peaks overlapped (595) and non-overlapped (4,511) with H3K27me3 sites in *SUZ12* KO cells. We found that those H3K18ub peaks that overlapped with H3K27me3 sites showed a higher increase in H3K18ub signal compared to those not overlapped with H3K27me3 sites following knockout of *SUZ12*. Moreover, 24.03% of the 595 H3K18ub peaks that overlapped with H3K27me3 sites increased greater than 4-fold, while only 0.40% of the 4,511 non-overlapping H3K18ub peaks exhibited a 4-fold or greater increase (Figure S6C in Supporting Information). We also examined the distribution of H3K18ub peaks with elevated signal that overlapped with H3K27me3 sites in *SUZ12* KO cells and found that the proportion of overlapping peaks increased with cut-off value, reaching 88.82% among peaks with a 4-fold or greater signal intensity compared to WT (Figure 4D). These data thus reveal that the loss of H3K27me3 marks leads to an increase in H3K18ub signal preferentially in previously marked H3K27me3 loci.

To further investigate whether the increased H3K18ub peaks were preferentially located at DNA hyper-methylated loci in the *SUZ12* KO genome, we analyzed the distribution of H3K18ub peaks with elevated signal that overlapped with hyper-DMRs in *SUZ12* KO cells. The results showed that the proportion of H3K18ub peaks which overlapped with hyper-DMRs also increased commensurately with fold-change cutoff (Figure 4E). Examination of individual loci revealed that the hyper-DMRs with enhanced H3K18ub signals in the *SUZ12* KO genome exhibited an obviously higher level of H3K27me3 modification in WT cells (Figure 4F and G). Taken together, these results indicate that depletion of H3K27me3 marks induces an increase in H3K18ub modification and DNA hyper-methylation, preferentially at previously marked H3K27me3 loci.

H3K27me3 modification inhibits UHRF1 E3 ubiquitin ligase activity towards H3

The above results suggest that H3K27me3 modification may negatively regulate DNA methylation levels through inhibition of H3 ubiquitination. Therefore, we tested whether H3K27me3 marks interfered with UHRF1 binding to nucleosomes or directly inhibited its E3 ubiquitin ligase activity towards H3. To this end, we performed *in vitro* pull-down experiments using biotinylated recombinant H3.1 nucleosomes or H3.1 nucleosomes tri-methylated at H3K27 with full length UHRF1 protein. These assays showed that nucleosomes with or without H3K27me3 modification pulled down UHRF1 with no detectable preference (Figure

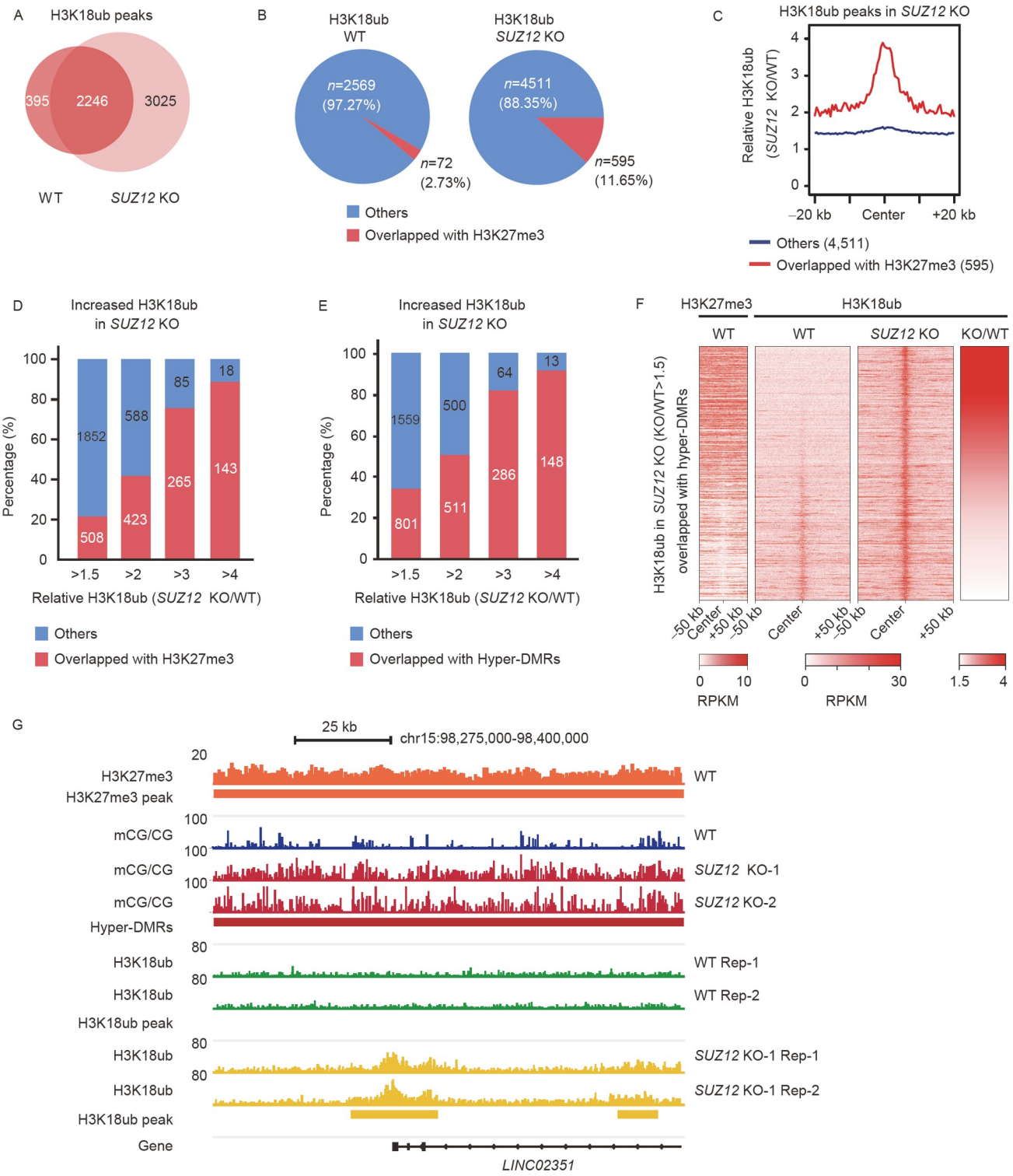

Figure 4 H3K18ub marks increase at previously marked H3K27me3 sites in the absence of H3K27me3. A, Venn diagram depicting the overlap of H3K18ub peaks in WT and *SUZ12* KO HeLa cells. B, Pie chart shows the distribution of H3K18ub peaks that overlapped with H3K27me3 marked sites in WT and *SUZ12* KO HeLa cells. *P*=2.7e-140 (Fisher's exact test). C, Profiles of the average KO/WT ratios of H3K18ub signals (RPKM) in H3K18ub peaks that overlapped with H3K27me3 sites (red) or non-overlapped with H3K27me3 sites (blue) in *SUZ12* KO HeLa cells. D, The distribution of increased H3K18ub peaks that overlapped or non-overlapped with H3K27me3 sites in *SUZ12 KO* cells at different fold-change cut-offs. E, The distribution of increased H3K18ub peaks that overlapped or non-overlapped with hyper-DMRs in *SUZ12 KO* cells at different fold-change cut-offs. F, Heatmaps representing the signal intensities of H3K27me3, H3K18ub, and KO/WT ratios of 801 H3K18ub peaks that overlapped with hyper-DMRs at a cut-off >1.5 in *SUZ12* KO HeLa cells. G, Genome browser showing the increase of H3K18ub modification at previously marked H3K27me3 hyper-DMRs. The overlapping H3K18ub peaks of two replicates are used in A–G, and the merged H3K18ub ChIP-seq data of two replicates are shown in C–F. The merged DMRs of two clones are used in E and F.

5A), indicating that H3K27me3 modification do not affect UHRF1 binding to nucleosomes.

Next, we performed *in vitro* ubiquitination reactions using full length UHRF1 protein and biotinylated H3.1 nucleosomes with or without tri-methylation at H3K27. The results clearly showed that UHRF1-mediated histone H3 ubiquitination activity (H3K18ub modification) was lower toward nucleosomes bearing H3K27me3 modification compared with that toward unmodified nucleosomes (Figure 5B). These results indicate that H3K27me3 modification can directly inhibit UHRF1 E3 ubiquitin ligase activity towards H3.

DISCUSSION

In this study, we uncover a mechanism by which H3K27me3 modification antagonizes DNA methylation via inhibition of UHRF1-mediated H3 ubiquitination, thereby revealing cross-talk between two repressive epigenetic modification systems through a third, transient, ubiquitination mark on H3. In H3K27me3 marked sites, H3K27me3 modification inhibits UHRF1-mediated H3 ubiquitination, and thus DNMT1 recruitment and activation are attenuated. Therefore, H3K27me3 marked sites maintain relatively low levels of DNA methylation (Figure 5C, left panel). Outside of H3K27me3 marked sites, UHRF1 can efficiently catalyze ubiquitination on H3, resulting in DNMT1 recruitment and activation for proper DNA methylation (Figure 5C, right panel).

As shown in this study, H3K27me3 does not affect UHRF1 binding to nucleosome, so how it inhibits the E3 ligase activity of UHRF1? UHRF1 is a multi-domain protein, which binds to hemi-mCpG via a SRA domain, cooperatively recognizes histone H3 tail and di-/trimethylation of Lys-9 (H3K9me2/3) through its linked tandem-tudor domain and plant homeodomain (TTD-PHD), and exhibits the E3 ubiquitin ligase activity via its C-terminal RING domain regulated by its N-terminal ubiquitin-like (UBL) domain (Arita et al., 2008; Arita et al., 2012; Hashimoto et al., 2008; Ming et al., 2021; Rothbart et al., 2012). The recruitment of DNMT1 to newly replicated chromatin critically depends on the ubiquitination of Lys-18 and Lys-23 in histone H3 mediated by UHRF1, while the E3 activity of UHRF1 is allosteric

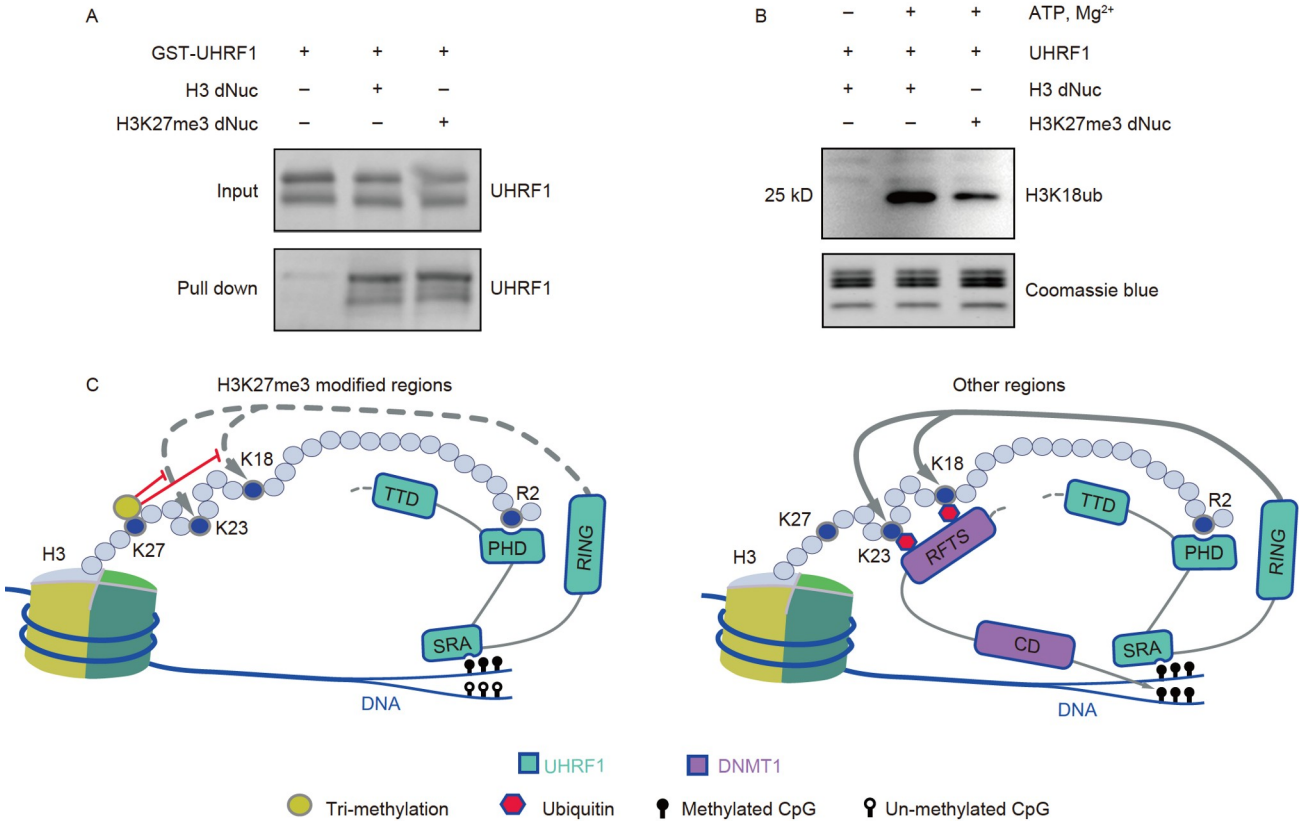

Figure 5 H3K27me3 modification inhibits UHRF1 E3 ubiquitin ligase activity towards H3. A, Biotinylated recombinant mono-nucleosome H3.1 dNuc or H3.1K27me3 dNuc immobilized on streptavidin-coated beads is used to pull down UHRF1. Unbound UHRF1 (Input) and pull-down samples are analyzed by western blot. B, UHRF1 *in vitro* ubiquitination reactions with the indicated H3.1 dNuc or H3.1K27me3 dNuc mono-nucleosome substrate. Ubiquitinated H3 is analyzed by western blot using H3K18ub antibody, and Coomassie blue staining is used for protein loading control. C, A model for H3K27me3 modification in shaping the DNA methylome by inhibition of UHRF1-mediated H3 ubiquitination. In H3K27me3 marked regions, H3K27me3 inhibits UHRF1-mediated H3 ubiquitination, thus attenuating DNMT1 recruitment and activation, resulting in decreased DNA methylation. In H3K27me3 unmarked regions, UHRF1 can catalyze ubiquitination on H3 to recruit and activate DNMT1 for proper DNA methylation.

regulated by the chromatin substrate or by inter-domain contacts within the protein (Nishiyama et al., 2013; Qin et al., 2015). Foster et al. suggest that chromatin structure may influence UHRF1 activity, because the higher activity of UHRF1-mediated histone H3 ubiquitination in the presence of 12 arrays of nucleosome is shown than in the presence of shorter substrates (DaRosa et al., 2018; Foster et al., 2018). The activity of chromatin modifying enzymes to be affected by existing chromatin modification has been previously documented. For example, methylation of H4 Arg 3 by PRMT1 can facilitate subsequent acetylation of H4 tails by p300 (Wang et al., 2001); H3K36me3 can inhibit H3K27 methylation by blocking the histone methyltransferase (HMTase) activity of full-length PHF1-PRC2 even though this complex has higher binding affinity on nucleosomes (Choi et al., 2017; Finogenova et al., 2020). It is likely that the tri-methylation of H3K27 may block an active UHRF1 conformation for ubiquitination of Lys-18 and Lys-23 in histone H3, which is an interesting direction warranting future investigation.

Our findings do not exclude the possibility that other mechanisms may also be involved in regulating hypo-methylation at H3K27me3 marked sites in a cell type-specific manner. For example, several mechanisms may cooperate to regulate hypo-methylation at DNA methylation valleys (DMVs) which enrich H3K27me3 (Grosswendt et al., 2020; Li et al., 2018b). Grosswendt et al. report that three PRC components (EED, RNF2 and KDM2B) contribute to the protection of DMV from hyper-methylation in mouse Epiblast (Grosswendt et al., 2020). In addition, Li et al. reported that Polycomb was required for the maintenance of DMV hypo-methylation in mESCs, likely through ten-eleven translocation (TET) proteins (Li et al., 2018b). We analyzed changes in DNA methylation at previously marked H3K27me3 sites in *Tet* TKO and *Suz12* KO mESCs (Lu et al., 2014) and found that *Tet* TKO cells exhibited an increase of DNA methylation at previously marked H3K27me3 sites, although smaller than that seen in *Suz12* KO (Figure S7 in Supporting Information). Therefore, TET proteins, which are highly expressed in mESCs, contribute to the hypo-methylation of Polycomb targeted DMVs together with H3K27me3-H3K18ub-UHRF1 axis (Li et al., 2018b). In contrast, the H3K27me3-H3K18ub-UHRF1 axis may play a more general role at all H3K27me3 marked sites. The expression and activity of TET proteins and DNMT3 proteins are very low in HeLa cells (Ming et al., 2020; Palii et al., 2008). Therefore, the mechanism discovered in the current study may exert a more pivotal regulatory effect on DNA methylation at H3K27me3 marked sites in somatic cells with low levels of TET and DNMT3 proteins, such as HeLa cells, than in mESCs.

Although DNA methylation and H3K27me3 modification are both involved in the establishment and maintenance of epigenetic gene silencing, it is believed that DNA methylation is more stable than H3K27me3 (Bird, 2002; Rose and Klose, 2014). DNA methylation is a defining feature of mammalian cellular identity and serves as the basis for the developmental stage- and cell-type specific epigenetic memory (Bird, 2002; Hon et al., 2013; Ziller et al., 2013). H3K27me3 modification typically marks the regulatory elements in a poised state, which enable quick induction of gene expression upon stimuli (Bernstein et al., 2006). Yang et al. showed that there could be a switch between H3K27me3 and DNA methylation in silencing key developmental genes at different stages. The H3K27me3 in embryonic cells enables regulated developmental plasticity of gene expression, while the DNA methylation in extra-embryonic ectoderm (ExE) cells set the permanent restriction of gene expression (Yang et al., 2018). In addition, Xie et al. found that during the process of human embryonic stem cell differentiation, promoters of genes transcribed during the early developmental stages were preferentially marked by H3K27me3, whereas by contrast, promoters for genes expressed preferentially in the later stages often primarily employed DNA methylation for repression (Xie et al., 2013).

Thus, the antagonism between these two modes of regulation facilitates activation of the correct gene expression programs during development to ensure lineage stability and phenotypic plasticity of cells, tissues, and species (Meehan and Pennings, 2017; Reddington et al., 2013). Previous studies have reported that DNA methylation has a negative effect on PRC2 binding to chromatin which constrains PRC2 targeting and the spread of H3K27me3 (Brinkman et al., 2012; Reddington et al., 2013; Wu et al., 2010). In this study, we reveal that H3K27me3 has a major role in constraining DNA methylation level by inhibiting UHRF1-mediated H3 ubiquitination. This discovery will significantly advance our understanding of the division and cooperation between H3K27me3 and DNA methylation, the two repressive chromatin modifications for determination of cell fate essential for development and tissue homeostasis.

MATERIALS AND METHODS

Cell culture and antibodies

HeLa-S3 cells were grown in Dulbecco's Modified Eagle's Medium (DMEM) (Gibco, USA) supplemented with 10% fetal bovine serum and 1% penicillin/streptomycin. E14Tg2a mESCs were cultured on 0.2% gelatin-coated plates in DMEM supplemented with 15% fetal bovine serum, 1% penicillin/streptomycin, 1% nonessential amino acid, 1% sodium pyruvate, β-mercaptoethanol and 1000 U/mL LIF (ESGRO, Millipore, USA).

Antibodies used in this study were H3K27me3 (Cell Signaling Technology, 9733, USA), UHRF1 (Santa Cruz, USA,

373750 for WB; Active Motif, 61341 for IF), H3K23ub (Abcam, UK), H3K18ub (generated in this study, see below for details), H3 (Abcam, UK), Tubulin (Sigma, T9026, USA) and SUZ12 (Cao et al., 2002).

Generation of KO cells

SUZ12 or Suz12 KO cells and *Uhrf1* KO cells were generated by large fragment deletion using dual guide RNAs through CRISPR/Cas9. E14 or HeLa cells were transfected with pX330 vectors encoding Cas9 and guide RNAs for *SUZ12*, *Suz12* or *Uhrf1* together with one other vector encoding puromycin resistance gene using lipid-based transfection reagent (Lipo3000, Invitrogen, USA). 24 h later, the cells were sub-cultured to a low density and selected with 2 μg mL^{-1} puromycin for 48 h. Viable clones were grown larger and picked up for knock out analysis. Positive clones were verified using PCR for genotyping and confirmed by western blots.

Generation and characterization of H3K18ub rabbit polyclonal antibody

Polyclonal antibodies against histone H3 ubiquitylated at Lys18 (H3K18ub) were generated by Jingjie PTM BioLab (Hangzhou) Co. Ltd (China). The two ubiquitylated peptides (CGKAPR-[LRGG] K-QLAT and GKAPR-[LRGG] K-QLATKC) and one unmodified peptide (GKAPRKQ-LATKC) were synthesized. The ubiquitylated peptides conjugated with keyhole limpet hemocyanin (KLH) were injected into three rabbits for immunization. After 55 days, the antisera from three rabbits were collected and detected by ELISA using the two ubiquitylated peptides and the corresponding unmodified peptide. The positive antisera were further screened by western blot using 20 μg crude proteins from Jurkat cells. Three antiserums were purified by affinity chromatography. After purification, we got Ab1, Ab2 and Ab3. The three antibodies were tested by ELISA, dot blot and western blot. According to these results, Ab2 showed the best specificity to H3K18ub and chosen for further validation shown in this study.

Plasmids and protein

All proteins used in this study align to the major human variant (UHRF1, Genebank ID: 586798168; H3.1, Genebank ID: 4504285). Full-length UHRF1 was cloned into a modified pMCSG7 vector as an N-terminal His-MBP fusion separated by a TEV cleavage site. Single colonies containing the expressing plasmid were picked and grown in LB with ampicillin (100 μg mL^{-1}) at 37°C until the OD600 reached 0.6–0.8. The temperature was then lowered to 16°C, isopropyl β-D-1-thiogalactopyranoside (IPTG) was added to a final concentration of 0.1 mmol L^{-1}, and cultures were incubated overnight with shaking. Cells were collected by centrifugation and resuspended in binding buffer (20 mmol L^{-1} NaH_2PO_4 at pH 7.4, 500 mmol L^{-1} NaCl, 20 mmol L^{-1} imidazole, 5% Glycerol) with 1 mmol L^{-1} PMSF. Cells were lysed by the addition of lysozyme (30 minutes on ice), followed by sonication on ice (300 W, on 5 s, pause 10 s, total 10 min). Insoluble material was then cleared by centrifugation (20,000*g*, 60 min, 4°C). The supernatant was filtered with 0.45 μm filter and applied to Ni Sepharose 6 Fast Flow resin (GE Healthcare, USA) equilibrated in binding buffer. The resin and bound protein were washed with at least 10 bed volumes of binding buffer, followed by elution of His-tagged proteins in five bed volumes of elution buffer (0.5 mol L^{-1} NaCl, 20 mmol L^{-1} NaH_2PO_4, 250 mmol L^{-1} imidazole, 5% Glycerol, pH 7.4). Proteins were cleaved by TEV protease to remove the His-MBP tag from UHRF1 in dialysis tubing (SnakeSkin, 10K MWCO, Thermo Fisher, USA), and dialyzed overnight at 4°C into TEV cleavage buffer (50 mmol L^{-1} Tris at pH 8.0, 1 mmol L^{-1} DTT, 0.5 mmol L^{-1} EDTA). Finally, cleaved UHRF1 was concentrated and snap frozen.

Ubiquitination assay

Ubiquitination assay was performed as described previously with minor modification (Vaughan et al., 2018). Briefly, ubiquitination reactions were performed in 20 μL ubiquitin assay buffer (20 mmol L^{-1} Tris HCl at pH 7.4, 100 mmol L^{-1} NaCl, 5 mmol L^{-1} $MgCl_2$, and 2.5 mmol L^{-1} DTT) for 60 min at 37°C. The ubiquitin machinery, including 200 nmol L^{-1} E1 (UBE1, BostonBiochem, USA), 1 μmol L^{-1} E2 (UBCH5A, BostonBiochem, USA), 1.5 μmol L^{-1} E3 (UHRF1) and 10 μmol L^{-1} ubiquitin (FLAG-ub, BostonBiochem, USA) were charged with the addition of ATP (5 mmol L^{-1}). Next, 0.5 μmol L^{-1} designer nucleosomes (dNucs) were added. Biotinylated recombinant human mono-nucleosomes H3.1 dNuc and H3.1K27me3 dNuc were purchased from Epicypher (USA). Reactions were quenched by the addition of SDS loading buffer to a final concentration of 1×. Reactions were separated by SDS/PAGE and immunoblotted with the antibodies indicated. Blots shown are representative of at least two independent replicates.

Immuno-precipitation and *in vitro* pull-down

For immuno-precipitation, about 3×10^7 HeLa cells were collected and washed twice by PBS, followed by incubating on ice for 30 min with 600 μL low salt buffer (20 mmol L^{-1} Tris HCl pH 7.9, 1.5 mmol L^{-1} $MgCl_2$, 0.2 mmol L^{-1} EDTA, 10 mmol L^{-1} NaCl, 0.5 mmol L^{-1} DTT, 10% glycerol) supplemented with 0.2% Triton X-100, 100 U mL^{-1} Cryonase nuclease (Takara, Japan), 1× protease inhibitor cocktail.

600 μL high salt buffer (20 mmol L^{-1} Tris HCl pH 7.9, 1.5 mmol L^{-1} $MgCl_2$, 0.2 mmol L^{-1} EDTA, 1 mol L^{-1} NaCl, 0.5 mmol L^{-1} DTT, 10% glycerol) supplemented with 1× protease inhibitor cocktail was added before incubation on ice for an additional 30 min. After centrifugation, the supernatant was pre-cleaned with Protein A Dynabeads for 2 h and then incubated with Protein A Dynabeads pre-linked with antibody against H3K27me3 overnight at 4°C. Beads were then washed five times with wash buffer (20 mmol L^{-1} Tris HCl pH 7.9, 500 mmol L^{-1} NaCl, 0.5 mmol L^{-1} DTT, 0.1% Triton X-100). Beads were boiled in 1× SDS loading buffer for immuno-blotting analysis.

Pull-down assays were performed in pull-down buffer (25 mmol L^{-1} Tris HCl at pH 7.5, 300 mmol L^{-1} NaCl, 0.5% BSA, 0.1% Nonidet P-40) (Vaughan et al., 2018). For each nucleosome pull-down, 5 μL streptavidin-coated beads (Pierce, USA) were incubated with 100 nmol L^{-1} biotinylated recombinant human mono-nucleosomes H3.1 recombinant dNuc or H3.1K27me3 dNuc for 30 min at room temperature. Beads were washed twice in pull-down buffer. UHRF1 (1 μmol L^{-1}) was incubated with conjugated beads in pull-down buffer (50 μL) overnight at 4°C. Unbound UHRF1 was collected for analysis as an input control. Beads were then washed 3 times in pull-down buffer and boiled in 100 μL of 1× SDS loading buffer.

ChIP-seq

Cells were crosslinked with 1% formaldehyde for 5 min. After quenching with 125 mmol L^{-1} glycine, the cells were harvested and digested by 2 U μL^{-1} MNase (NEB, USA) at 37°C for 20 min to produce soluble chromatin with DNA fragments in the range of 150–300 bp. The lysates were then sonicated for 5 min (30 s on/30 s off) using Bioruptor Sonicator (Diagenode, USA) and centrifuged at 21,130*g* for 10 min. The supernatants were collected and the chromatin content was incubated with Protein A and Protein G Dynabeads pre-linked with antibodies against H3K18ub overnight at 4°C. Bound chromatin was washed extensively, then eluted and reverse-crosslinked at 65°C overnight using elution buffer. After being treated by RNase A and proteinase K, the samples were extracted by phenol: chloroform and precipitated with ethanol in the presence of linear acrylamide. After dissolving in nuclease free TE buffer, the samples are ready for sequencing library construction.

WGBS

Genomic DNA (500 ng) was added with 1% lambda DNA and sheared by Bioruptor sonicator to achieve DNA fragments with peak size around 350 bp. The methylated Illumina sequencing adaptors were added according to the manufacturer's instruction (NEBNext Ultra DNA Library Prep Kit for Illumina, NEB). EpiTect fast bisulfite conversion kit (Qiagen, Germany) was used for bisulfite conversion. The reaction time for both of the two conversion steps was 20 min. Then the WGBS libraries were amplified using KAPA HiFi HotStart Uracil+ ReadyMix (Roche, USA). The libraries were then sequenced by 150 bp pair-end sequencing on a NovaSeq instrument (Illumina, USA).

RNA-seq

RNA samples were extracted by Trizol (Life Tech, USA). Barcoded RNA-seq libraries were constructed using NEBNext ultra II directional RNA library prep kit for Illumina according to the manufacturer's instructions (NEB).

Quality control and read preprocessing

Sequencing quality and adapter-contamination were checked by FastQC and MultiQC (Ewels et al., 2016). Raw sequencing reads of WGBS, ChIP-seq and RNA-seq libraries in this study were trimmed to remove the adapter-contaminated and low-quality reads using Trim Galore (Version 0.4.4_dev) with default parameters. Clean reads were used for the following analysis.

WGBS analysis

The sequencing reads were aligned to the reference genome (hg38/mm10) using Bismark v0.19.0. Then the methylation level and coverage depth for each cytosines were calculated using Bismark (Krueger and Andrews, 2011). HeLa and E14 cell DNA reads were successfully bisulfite-converted (>99.8%). The average DNA methylation level at H3K27me3 peaks was summarized by the "plotHeatmap" function in the deepTools suit (Ramírez et al., 2016). Methylation levels from both strands were combined for each of the CpG sites. The differential DNA methylation was calculated as the difference in weighted methylation level between wild type and *SUZ12* KO (Schultz et al., 2012). Regions non-overlapped with H3K27me3 peaks in the genome were defined by the "complement" function in the BEDTools v2.27.1 suit (Quinlan and Hall, 2010). Then we applied a violin plot to exemplify different weighted methylation level of these two types of regions by the R package ggplot2. Multi-columns heatmaps were produced with normalized sequencing coverages or methylation levels that were averaged in 50 or 100 bp bins around the center of peaks by EnrichedHeatmap package (Gu et al., 2018). DMRs (differential methylation regions) analysis was performed by methpipe-3.4.3. HeLa/E14 DMRs with more than 5/10 CpGs and at least 3/5 significantly differentially methylated CpGs were selected, respectively (Song et al., 2013). DMRs in two replicates of KO were merged in the following analysis. In

addition, HeLa DMRs were merged if the distance was less than 160 kb.

ChIP-seq analysis

Clean reads of H3K27me3 ChIP-seq were aligned to the human reference genome (hg38) and mouse reference genome (mm10), respectively, using Bowtie2 with default parameters (Langmead and Salzberg, 2012). Unmapped reads, multiple mapped reads and PCR duplicates were removed by samtools and Picard (Li et al., 2009). Read counts were normalized with the RPKM method with a 10 bp window by deepTools. HeLa H3K18ub peaks were called using MACS2 with the parameters: -broad -g 2.9e9 -q 0.05 -f BAMPE -nomodel -extsize 147 -B (Zhang et al., 2008). HeLa H3K18ub peaks were then merged if the distance was less than 5 kb and filtered if shorter than 800 bp. The HeLa H3K18ub peaks existed in both replicates were used for following analysis. The HeLa H3K18ub signal intensity tracks of *SUZ12* KO and WT were calculated with the RPKM value using merged bam files of two replicates. Finally, we identified 2,641 H3K18ub peaks in WT and 5,106 H3K18ub peaks in *SUZ12* KO HeLa cells. Among the 2,641 H3K18ub peaks in WT cells, 2,246 peaks were overlapped with peaks in *SUZ12* KO cells, and among the 5,106 H3K18ub peaks in *SUZ12* KO HeLa cells, 2,081 peaks were overlapped with peaks in WT cells, while 3,025 peaks were newly emerged peaks in the absence of H3K27me3. The E14 H3K18ub peaks were called using SICER with the parameters: -window size 200 -gap size 200. The E14 H3K18ub peaks existed in both replicates were used for following analysis. The read counts of each peaks were summarized by featureCounts and RPKM of each peak was calculated using merged bam files of two replicates (Liao et al., 2014). E14 H3K27me3 peaks were called by SICER with parameters: -window size 200 -gap size 600. H3K18ub peaks annotation of E14 and HeLa were performed with ChIPseeker and BEDTools (Quinlan and Hall, 2010; Yu et al., 2015).

RNA-seq analysis

Gene expression of wild type HeLa cells and *SUZ12* KO HeLa cells strand specific RNA-seq data were quantified using Salmon (version 0.12.0) with parameters: -l ISR -seqBias -gcBias -posBias (Patro et al., 2017). Then DESeq2 was used to normalize read counts of each genes and to perform differential expression analysis (Love et al., 2014). The up-regulated and down-regulated genes were identified by comparing two replicates of wild type with two replicates of *SUZ12* KO HeLa cell samples using a two-fold change threshold and adjusted p value <0.01. Genes overlapped with the H3K27me3 or DMRs were identified by the BEDTools intersect function with parameter: -f 0.01.

Published datasets used in this study

Published H3K27me3 ChIP-seq data were downloaded from GEO datasets: HeLa cell from GSE43094; E14 cell from GSE23943. We downloaded mouse WGBS and H3K27me3 ChIP-seq raw data sets of multiple organs from GEO database for Figure 1A: liver (GSE83063; GSE82780), kidney (GSE82791; GSE82451) and lung (GSE82362; GSE82669). The human raw data of three organs were downloaded from "UCSD Human Reference Epigenome Mapping Project" (GSE16256). E14 WT and *Tet* TKO raw data were downloaded from GEO datasets (GSE56986).

DATA AVAILABILITY

All WGBS, ChIP-seq, and RNA-seq datasets are deposited in the NCBI Gene Expression Omnibus (GEO) database under accession code GSE159043.

Compliance and ethics *The author(s) declare that they have no conflict of interest.*

Acknowledgements *This work was supported by the National Key Research and Development Program of China (2018YFA0107001, 2018YFC1004000), the CAS Project for Young Scientists in Basic Research (YSBR-012), and the National Natural Science Foundation of China (32070607). We thank Dr. Jiemin Wong from East China Normal University for the UHRF1 expression plasmid.*

References

Amir, R.E., Van den Veyver, I.B., Wan, M., Tran, C.Q., Francke, U., and Zoghbi, H.Y. (1999). Rett syndrome is caused by mutations in X-linked MECP2, encoding methyl-CpG-binding protein 2. Nat Genet 23, 185–188.

Aran, D., and Hellman, A. (2013). DNA methylation of transcriptional enhancers and cancer predisposition. Cell 154, 11–13.

Aran, D., Sabato, S., and Hellman, A. (2013). DNA methylation of distal regulatory sites characterizes dysregulation of cancer genes. Genome Biol 14, R21.

Arita, K., Ariyoshi, M., Tochio, H., Nakamura, Y., and Shirakawa, M. (2008). Recognition of hemi-methylated DNA by the SRA protein UHRF1 by a base-flipping mechanism. Nature 455, 818–821.

Arita, K., Isogai, S., Oda, T., Unoki, M., Sugita, K., Sekiyama, N., Kuwata, K., Hamamoto, R., Tochio, H., Sato, M., et al. (2012). Recognition of modification status on a histone H3 tail by linked histone reader modules of the epigenetic regulator UHRF1. Proc Natl Acad Sci USA 109, 12950–12955.

Barau, J., Teissandier, A., Zamudio, N., Roy, S., Nalesso, V., Hérault, Y., Guillou, F., and Bourc'his, D. (2016). The DNA methyltransferase DNMT3C protects male germ cells from transposon activity. Science 354, 909–912.

Bartke, T., Vermeulen, M., Xhemalce, B., Robson, S.C., Mann, M., and Kouzarides, T. (2010). Nucleosome-interacting proteins regulated by DNA and histone methylation. Cell 143, 470–484.

Bell, R.E., Golan, T., Sheinboim, D., Malcov, H., Amar, D., Salamon, A., Liron, T., Gelfman, S., Gabet, Y., Shamir, R., et al. (2016). Enhancer methylation dynamics contribute to cancer plasticity and patient mortality. Genome Res 26, 601–611.

Bernstein, B.E., Mikkelsen, T.S., Xie, X., Kamal, M., Huebert, D.J., Cuff,

J., Fry, B., Meissner, A., Wernig, M., Plath, K., et al. (2006). A bivalent chromatin structure marks key developmental genes in embryonic stem cells. Cell 125, 315–326.
Bernstein, B.E., Stamatoyannopoulos, J.A., Costello, J.F., Ren, B., Milosavljevic, A., Meissner, A., Kellis, M., Marra, M.A., Beaudet, A. L., Ecker, J.R., et al. (2010). The NIH roadmap epigenomics mapping consortium. Nat Biotechnol 28, 1045–1048.
Bird, A. (2002). DNA methylation patterns and epigenetic memory. Genes Dev 16, 6–21.
Bostick, M., Kim, J.K., Esteve, P.O., Clark, A., Pradhan, S., and Jacobsen, S.E. (2007). UHRF1 plays a role in maintaining DNA methylation in mammalian cells. Science 317, 1760–1764.
Brinkman, A.B., Gu, H., Bartels, S.J.J., Zhang, Y., Matarese, F., Simmer, F., Marks, H., Bock, C., Gnirke, A., Meissner, A., et al. (2012). Sequential ChIP-bisulfite sequencing enables direct genome-scale investigation of chromatin and DNA methylation cross-talk. Genome Res 22, 1128–1138.
Brocks, D., Assenov, Y., Minner, S., Bogatyrova, O., Simon, R., Koop, C., Oakes, C., Zucknick, M., Lipka, D.B., Weischenfeldt, J., et al. (2014). Intratumor DNA methylation heterogeneity reflects clonal evolution in aggressive prostate cancer. Cell Rep 8, 798–806.
Brookes, E., and Shi, Y. (2014). Diverse epigenetic mechanisms of human disease. Annu Rev Genet 48, 237–268.
Cao, R., Wang, L., Wang, H., Xia, L., Erdjument-Bromage, H., Tempst, P., Jones, R.S., and Zhang, Y. (2002). Role of histone H3 lysine 27 methylation in Polycomb-group silencing. Science 298, 1039–1043.
Cao, R., and Zhang, Y. (2004). The functions of E(Z)/EZH2-mediated methylation of lysine 27 in histone H3. Curr Opin Genet Dev 14, 155–164.
Chen, Z., and Zhang, Y. (2020). Role of mammalian DNA methyltransferases in development. Annu Rev Biochem 89, 135–158.
Chittock, E.C., Latwiel, S., Miller, T.C.R., and Müller, C.W. (2017). Molecular architecture of polycomb repressive complexes. Biochem Soc Trans 45, 193–205.
Choi, J., Bachmann, A.L., Tauscher, K., Benda, C., Fierz, B., and Müller, J. (2017). DNA binding by PHF1 prolongs PRC2 residence time on chromatin and thereby promotes H3K27 methylation. Nat Struct Mol Biol 24, 1039–1047.
The ENCODE Project Consortium, (2012). An integrated encyclopedia of DNA elements in the human genome. Nature 489, 57–74.
DaRosa, P.A., Harrison, J.S., Zelter, A., Davis, T.N., Brzovic, P., Kuhlman, B., and Klevit, R.E. (2018). A bifunctional role for the UHRF1 UBL domain in the control of hemi-methylated DNA-dependent histone ubiquitylation. Mol Cell 72, 753–765.e6.
Disteche, C.M., and Berletch, J.B. (2015). X-chromosome inactivation and escape. J Genet 94, 591–599.
Elhamamsy, A.R. (2017). Role of DNA methylation in imprinting disorders: an updated review. J Assist Reprod Genet 34, 549–562.
Elliott, E.N., Sheaffer, K.L., and Kaestner, K.H. (2016). The '*de novo*' DNA methyltransferase Dnmt3b compensates the Dnmt1-deficient intestinal epithelium. eLife 5, e12975.
Ewels, P., Magnusson, M., Lundin, S., and Käller, M. (2016). MultiQC: summarize analysis results for multiple tools and samples in a single report. Bioinformatics 32, 3047–3048.
Finogenova, K., Bonnet, J., Poepsel, S., Schäfer, I.B., Finkl, K., Schmid, K., Litz, C., Strauss, M., Benda, C., and Müller, J. (2020). Structural basis for PRC2 decoding of active histone methylation marks H3K36me2/3. eLife 9, e61964.
Foster, B.M., Stolz, P., Mulholland, C.B., Montoya, A., Kramer, H., Bultmann, S., and Bartke, T. (2018). Critical role of the UBL domain in stimulating the E3 ubiquitin ligase activity of UHRF1 toward chromatin. Mol Cell 72, 739–752.e9.
Goll, M.G., and Bestor, T.H. (2005). Eukaryotic cytosine methyltransferases. Annu Rev Biochem 74, 481–514.
Grosswendt, S., Kretzmer, H., Smith, Z.D., Kumar, A.S., Hetzel, S., Wittler, L., Klages, S., Timmermann, B., Mukherji, S., and Meissner, A. (2020). Epigenetic regulator function through mouse gastrulation. Nature 584, 102–108.
Gu, Z., Eils, R., Schlesner, M., and Ishaque, N. (2018). EnrichedHeatmap: an R/Bioconductor package for comprehensive visualization of genomic signal associations. BMC Genom 19, 234.
Hagarman, J.A., Motley, M.P., Kristjansdottir, K., and Soloway, P.D. (2013). Coordinate regulation of DNA methylation and H3K27me3 in mouse embryonic stem cells. PLoS ONE 8, e53880.
Hashimoto, H., Horton, J.R., Zhang, X., Bostick, M., Jacobsen, S.E., and Cheng, X. (2008). The SRA domain of UHRF1 flips 5-methylcytosine out of the DNA helix. Nature 455, 826–829.
Hawkins, R.D., Hon, G.C., Lee, L.K., Ngo, Q.M., Lister, R., Pelizzola, M., Edsall, L.E., Kuan, S., Luu, Y., Klugman, S., et al. (2010). Distinct epigenomic landscapes of pluripotent and lineage-committed human cells. Cell Stem Cell 6, 479–491.
Hirabayashi, Y., Suzki, N., Tsuboi, M., Endo, T.A., Toyoda, T., Shinga, J., Koseki, H., Vidal, M., and Gotoh, Y. (2009). Polycomb limits the neurogenic competence of neural precursor cells to promote astrogenic fate transition. Neuron 63, 600–613.
Højfeldt, J.W., Laugesen, A., Willumsen, B.M., Damhofer, H., Hedehus, L., Tvardovskiy, A., Mohammad, F., Jensen, O.N., and Helin, K. (2018). Accurate H3K27 methylation can be established *de novo* by SUZ12-directed PRC2. Nat Struct Mol Biol 25, 225–232.
Hon, G.C., Hawkins, R.D., Caballero, O.L., Lo, C., Lister, R., Pelizzola, M., Valsesia, A., Ye, Z., Kuan, S., Edsall, L.E., et al. (2012). Global DNA hypomethylation coupled to repressive chromatin domain formation and gene silencing in breast cancer. Genome Res 22, 246–258.
Hon, G.C., Rajagopal, N., Shen, Y., McCleary, D.F., Yue, F., Dang, M.D., and Ren, B. (2013). Epigenetic memory at embryonic enhancers identified in DNA methylation maps from adult mouse tissues. Nat Genet 45, 1198–1206.
Ishiyama, S., Nishiyama, A., Saeki, Y., Moritsugu, K., Morimoto, D., Yamaguchi, L., Arai, N., Matsumura, R., Kawakami, T., Mishima, Y., et al. (2017). Structure of the Dnmt1 reader module complexed with a unique two-mono-ubiquitin mark on histone H3 reveals the basis for DNA methylation maintenance. Mol Cell 68, 350–360.e7.
Jain, D., Meydan, C., Lange, J., Claeys Bouuaert, C., Lailler, N., Mason, C. E., Anderson, K.V., and Keeney, S. (2017). *rahu* is a mutant allele of *Dnmt3c*, encoding a DNA methyltransferase homolog required for meiosis and transposon repression in the mouse male germline. PLoS Genet 13, e1006964.
Krueger, F., and Andrews, S.R. (2011). Bismark: a flexible aligner and methylation caller for Bisulfite-Seq applications. Bioinformatics 27, 1571–1572.
Langmead, B., and Salzberg, S.L. (2012). Fast gapped-read alignment with Bowtie 2. Nat Methods 9, 357–359.
Laugesen, A., Højfeldt, J.W., and Helin, K. (2019). Molecular mechanisms directing PRC2 recruitment and H3K27 methylation. Mol Cell 74, 8–18.
Li, E., and Zhang, Y. (2014). DNA methylation in mammals. Cold Spring Harbor Perspect Biol 6, a019133.
Li, H., Handsaker, B., Wysoker, A., Fennell, T., Ruan, J., Homer, N., Marth, G., Abecasis, G., and Durbin, R. (2009). The sequence alignment/map format and SAMtools. Bioinformatics 25, 2078–2079.
Li, Y., Zhang, Z., Chen, J., Liu, W., Lai, W., Liu, B., Li, X., Liu, L., Xu, S., Dong, Q., et al. (2018a). Stella safeguards the oocyte methylome by preventing *de novo* methylation mediated by DNMT1. Nature 564, 136–140.
Li, Y., Zheng, H., Wang, Q., Zhou, C., Wei, L., Liu, X., Zhang, W., Zhang, Y., Du, Z., Wang, X., et al. (2018b). Genome-wide analyses reveal a role of Polycomb in promoting hypomethylation of DNA methylation valleys. Genome Biol 19, 18.
Liao, Y., Smyth, G.K., and Shi, W. (2014). featureCounts: an efficient general purpose program for assigning sequence reads to genomic features. Bioinformatics 30, 923–930.
Lister, R., Pelizzola, M., Dowen, R.H., Hawkins, R.D., Hon, G., Tonti-Filippini, J., Nery, J.R., Lee, L., Ye, Z., Ngo, Q.M., et al. (2009). Human

DNA methylomes at base resolution show widespread epigenomic differences. Nature 462, 315–322.
Lister, R., Pelizzola, M., Kida, Y.S., Hawkins, R.D., Nery, J.R., Hon, G., Antosiewicz-Bourget, J., O'Malley, R., Castanon, R., Klugman, S., et al. (2011). Hotspots of aberrant epigenomic reprogramming in human induced pluripotent stem cells. Nature 471, 68–73.
Liu, X., Gao, Q., Li, P., Zhao, Q., Zhang, J., Li, J., Koseki, H., and Wong, J. (2013). UHRF1 targets DNMT1 for DNA methylation through cooperative binding of hemi-methylated DNA and methylated H3K9. Nat Commun 4, 1563.
Love, M.I., Huber, W., and Anders, S. (2014). Moderated estimation of fold change and dispersion for RNA-seq data with DESeq2. Genome Biol 15, 550.
Lu, F., Liu, Y., Jiang, L., Yamaguchi, S., and Zhang, Y. (2014). Role of Tet proteins in enhancer activity and telomere elongation. Genes Dev 28, 2103–2119.
Margueron, R., Li, G., Sarma, K., Blais, A., Zavadil, J., Woodcock, C.L., Dynlacht, B.D., and Reinberg, D. (2008). Ezh1 and Ezh2 maintain repressive chromatin through different mechanisms. Mol Cell 32, 503–518.
Margueron, R., and Reinberg, D. (2011). The Polycomb complex PRC2 and its mark in life. Nature 469, 343–349.
Meehan, R.R., and Pennings, S. (2017). Shoring up DNA methylation and H3K27me3 domain demarcation at developmental genes. EMBO J 36, 3407–3408.
Micheletti, R., Plaisance, I., Abraham, B.J., Sarre, A., Ting, C.C., Alexanian, M., Maric, D., Maison, D., Nemir, M., Young, R.A., et al. (2017). The long noncoding RNA *Wisper* controls cardiac fibrosis and remodeling. Sci Transl Med 9.
Ming, X., Zhang, Z., Zou, Z., Lv, C., Dong, Q., He, Q., Yi, Y., Li, Y., Wang, H., and Zhu, B. (2020). Kinetics and mechanisms of mitotic inheritance of DNA methylation and their roles in aging-associated methylome deterioration. Cell Res 30, 980–996.
Ming, X., Zhu, B., and Li, Y. (2021). Mitotic inheritance of DNA methylation: more than just copy and paste. J Genet Genom 48, 1–13.
Miró, X., Zhou, X., Boretius, S., Michaelis, T., Kubisch, C., Alvarez-Bolado, G., and Gruss, P. (2009). Haploinsufficiency of the murine polycomb gene *Suz12* results in diverse malformations of the brain and neural tube. Dis Model Mech 2, 412–418.
Murphy, P.J., Cipriany, B.R., Wallin, C.B., Ju, C.Y., Szeto, K., Hagarman, J. A., Benitez, J.J., Craighead, H.G., and Soloway, P.D. (2013). Single-molecule analysis of combinatorial epigenomic states in normal and tumor cells. Proc Natl Acad Sci USA 110, 7772–7777.
Nishiyama, A., Yamaguchi, L., Sharif, J., Johmura, Y., Kawamura, T., Nakanishi, K., Shimamura, S., Arita, K., Kodama, T., Ishikawa, F., et al. (2013). Uhrf1-dependent H3K23 ubiquitylation couples maintenance DNA methylation and replication. Nature 502, 249–253.
Okano, M., Bell, D.W., Haber, D.A., and Li, E. (1999). DNA methyltransferases Dnmt3a and Dnmt3b are essential for *de novo* methylation and mammalian development. Cell 99, 247–257.
Palii, S.S., Van Emburgh, B.O., Sankpal, U.T., Brown, K.D., and Robertson, K.D. (2008). DNA methylation inhibitor 5-Aza-2′-deoxycytidine induces reversible genome-wide DNA damage that is distinctly influenced by DNA methyltransferases 1 and 3B. Mol Cell Biol 28, 752–771.
Patro, R., Duggal, G., Love, M.I., Irizarry, R.A., and Kingsford, C. (2017). Salmon provides fast and bias-aware quantification of transcript expression. Nat Methods 14, 417–419.
Qin, W., Wolf, P., Liu, N., Link, S., Smets, M., La Mastra, F., Forné, I., Pichler, G., Hörl, D., Fellinger, K., et al. (2015). DNA methylation requires a DNMT1 ubiquitin interacting motif (UIM) and histone ubiquitination. Cell Res 25, 911–929.
Quinlan, A.R., and Hall, I.M. (2010). BEDTools: a flexible suite of utilities for comparing genomic features. Bioinformatics 26, 841–842.
Ramírez, F., Ryan, D.P., Grüning, B., Bhardwaj, V., Kilpert, F., Richter, A. S., Heyne, S., Dündar, F., and Manke, T. (2016). deepTools2: a next generation web server for deep-sequencing data analysis. Nucl Acids Res 44, W160–W165.
Reddington, J.P., Perricone, S.M., Nestor, C.E., Reichmann, J., Youngson, N.A., Suzuki, M., Reinhardt, D., Dunican, D.S., Prendergast, J.G., Mjoseng, H., et al. (2013). Redistribution of H3K27me3 upon DNA hypomethylation results in de-repression of Polycomb target genes. Genome Biol 14, R25.
Rose, N.R., and Klose, R.J. (2014). Understanding the relationship between DNA methylation and histone lysine methylation. Biochim Biophys Acta (BBA)-Gene Regulatory Mech 1839, 1362–1372.
Rothbart, S.B., Krajewski, K., Nady, N., Tempel, W., Xue, S., Badeaux, A. I., Barsyte-Lovejoy, D., Martinez, J.Y., Bedford, M.T., Fuchs, S.M., et al. (2012). Association of UHRF1 with methylated H3K9 directs the maintenance of DNA methylation. Nat Struct Mol Biol 19, 1155–1160.
Schmitz, R.J., Lewis, Z.A., and Goll, M.G. (2019). DNA methylation: shared and divergent features across eukaryotes. Trends Genet 35, 818–827.
Schultz, M.D., He, Y., Whitaker, J.W., Hariharan, M., Mukamel, E.A., Leung, D., Rajagopal, N., Nery, J.R., Urich, M.A., Chen, H., et al. (2015). Human body epigenome maps reveal noncanonical DNA methylation variation. Nature 523, 212–216.
Schultz, M.D., Schmitz, R.J., and Ecker, J.R. (2012). 'Leveling' the playing field for analyses of single-base resolution DNA methylomes. Trends Genet 28, 583–585.
Schwartzentruber, J., Korshunov, A., Liu, X.Y., Jones, D.T.W., Pfaff, E., Jacob, K., Sturm, D., Fontebasso, A.M., Quang, D.A.K., Tönjes, M., et al. (2012). Driver mutations in histone H3.3 and chromatin remodelling genes in paediatric glioblastoma. Nature 482, 226–231.
Sharif, J., Muto, M., Takebayashi, S.I., Suetake, I., Iwamatsu, A., Endo, T. A., Shinga, J., Mizutani-Koseki, Y., Toyoda, T., Okamura, K., et al. (2007). The SRA protein Np95 mediates epigenetic inheritance by recruiting Dnmt1 to methylated DNA. Nature 450, 908–912.
Simon, J.A., and Kingston, R.E. (2009). Mechanisms of polycomb gene silencing: knowns and unknowns. Nat Rev Mol Cell Biol 10, 697–708.
Song, Q., Decato, B., Hong, E.E., Zhou, M., Fang, F., Qu, J., Garvin, T., Kessler, M., Zhou, J., and Smith, A.D. (2013). A reference methylome database and analysis pipeline to facilitate integrative and comparative epigenomics. PLoS ONE 8, e81148.
Stadler, M.B., Murr, R., Burger, L., Ivanek, R., Lienert, F., Schöler, A., van Nimwegen, E., Wirbelauer, C., Oakeley, E.J., Gaidatzis, D., et al. (2011). DNA-binding factors shape the mouse methylome at distal regulatory regions. Nature 480, 490–495.
Tsumura, A., Hayakawa, T., Kumaki, Y., Takebayashi, S., Sakaue, M., Matsuoka, C., Shimotohno, K., Ishikawa, F., Li, E., Ueda, H.R., et al. (2006). Maintenance of self-renewal ability of mouse embryonic stem cells in the absence of DNA methyltransferases Dnmt1, Dnmt3a and Dnmt3b. Genes Cells 11, 805–814.
Vaughan, R.M., Dickson, B.M., Whelihan, M.F., Johnstone, A.L., Cornett, E.M., Cheek, M.A., Ausherman, C.A., Cowles, M.W., Sun, Z.W., and Rothbart, S.B. (2018). Chromatin structure and its chemical modifications regulate the ubiquitin ligase substrate selectivity of UHRF1. Proc Natl Acad Sci USA 115, 8775–8780.
Wang, H., Huang, Z.Q., Xia, L., Feng, Q., Erdjument-Bromage, H., Strahl, B.D., Briggs, S.D., Allis, C.D., Wong, J., Tempst, P., et al. (2001). Methylation of histone H4 at arginine 3 facilitating transcriptional activation by nuclear hormone receptor. Science 293, 853–857.
Wang, H., Yang, H., Shivalila, C.S., Dawlaty, M.M., Cheng, A.W., Zhang, F., and Jaenisch, R. (2013). One-step generation of mice carrying mutations in multiple genes by CRISPR/Cas-mediated genome engineering. Cell 153, 910–918.
Wang, Q., Yu, G., Ming, X., Xia, W., Xu, X., Zhang, Y., Zhang, W., Li, Y., Huang, C., Xie, H., et al. (2020). Imprecise DNMT1 activity coupled with neighbor-guided correction enables robust yet flexible epigenetic inheritance. Nat Genet 52, 828–839.
Wu, G., Broniscer, A., McEachron, T.A., Lu, C., Paugh, B.S., Becksfort, J., Qu, C., Ding, L., Huether, R., Parker, M., et al. (2012). Somatic histone H3 alterations in pediatric diffuse intrinsic pontine gliomas and non-brainstem glioblastomas. Nat Genet 44, 251–253.

Wu, H., Coskun, V., Tao, J., Xie, W., Ge, W., Yoshikawa, K., Li, E., Zhang, Y., and Sun, Y.E. (2010). Dnmt3a-dependent nonpromoter DNA methylation facilitates transcription of neurogenic genes. Science 329, 444–448.
Xie, W., Schultz, M.D., Lister, R., Hou, Z., Rajagopal, N., Ray, P., Whitaker, J.W., Tian, S., Hawkins, R.D., Leung, D., et al. (2013). Epigenomic analysis of multilineage differentiation of human embryonic stem cells. Cell 153, 1134–1148.
Yang, X., Hu, B., Hou, Y., Qiao, Y., Wang, R., Chen, Y., Qian, Y., Feng, S., Chen, J., Liu, C., et al. (2018). Silencing of developmental genes by H3K27me3 and DNA methylation reflects the discrepant plasticity of embryonic and extraembryonic lineages. Cell Res 28, 593–596.
Yu, G., Wang, L.G., and He, Q.Y. (2015). ChIPseeker: an R/Bioconductor package for ChIP peak annotation, comparison and visualization. Bioinformatics 31, 2382–2383.
Yu, J.R., Lee, C.H., Oksuz, O., Stafford, J.M., and Reinberg, D. (2019). PRC2 is high maintenance. Genes Dev 33, 903–935.
Yu, W., Zhang, F., Wang, S., Fu, Y., Chen, J., Liang, X., Le, H., Pu, W.T., and Zhang, B. (2017). Depletion of Polycomb repressive complex 2 core component EED impairs fetal hematopoiesis. Cell Death Dis 8, e2744.
Zhang, Y., Liu, T., Meyer, C.A., Eeckhoute, J., Johnson, D.S., Bernstein, B. E., Nusbaum, C., Myers, R.M., Brown, M., Li, W., et al. (2008). Model-based analysis of ChIP-Seq (MACS). Genome Biol 9, R137.
Zhao, X., and Wu, X. (2021). Polycomb-group proteins in the initiation and progression of cancer. J Genet Genom 48, 433–443.
Ziller, M.J., Gu, H., Müller, F., Donaghey, J., Tsai, L.T.Y., Kohlbacher, O., De Jager, P.L., Rosen, E.D., Bennett, D.A., Bernstein, B.E., et al. (2013). Charting a dynamic DNA methylation landscape of the human genome. Nature 500, 477–481.

SUPPORTING INFORMATION

The supporting information is available online at https://doi.org/10.1007/s11427-022-2155-0. The supporting materials are published as submitted, without typesetting or editing. The responsibility for scientific accuracy and content remains entirely with the authors.